Turkish Neurosurgery, 2004, Vol: 14, No: 1-2, 1-11

Surface Strain and Stress Analysis of the Mid-Cervical Vertebrae Bony Compartments: A Biomechanical Pilot Study

Orta Servikal Vertebra Kemik Bölümlerinin Gerilme ve Şekil Değiştirme Analizi: Biyomekanik Pilot Çalışma

Hakan BOZKUŞ[1]
Ergun BOZDAĞ[2]
Emin SÜNBÜLOĞLU[2]
Ercan TANYELİ[3]
Ali Çetin SARIOĞLU[1]
Murat HANCI[3]

1 Department of Neurosurgery, VKV Amerikan Hastanesi, Istanbul, Turkey
Institute of Science and Technology, Istanbul Technical University, Istanbul, Turkey
2 Department of Mechanical Engineering, Istanbul Technical University, Istanbul, Turkey
3 Cerrahpasa School of Medicine Istanbul University, Istanbul, Turkey

Received : 07.07.2003
Accepted : 03.11.2003

ABSTRACT

OBJECTIVE: This study provides preliminary information on stress distribution over the cervical spine in static physiologic loading conditions with the strain-gage technique. Limited numbers of in vitro studies have been conducted to investigate strain and stress patterns on the bony structure of the functional cervical spine unit by various techniques.

METHODS: In this pilot biomechanical study, strain gages were applied to the vertebral bodies and bilateral laminar sides of the C4, C5 and C6 levels in an occiput-T1 human cadaver model. Three different loading tests (axial compression, flexion and extension compressions) were conducted under static physiologic loading conditions.

RESULTS: The anterior vertebral body experienced compressive stress with axial compressive and flexion loadings and tensile stress with extension loading. Laminar stresses were tensile pattern during axial compressive loading while tensile and compressive stresses were equal during flexion and extension loadings.

CONCLUSION: The vertebral bodies adapt to each of the loadings with an expected compressive or tensile mechanic pattern as a one side fixed elastic beam in sagittal plane.

KEY WORDS: Biomechanics, cervical spine, strain, stress.

ÖZ

AMAÇ: Bu çalışma, boyun omurgasının statik fizyolojik yükleme durumundaki gerilme dağılımını strain-gage tekniği uygulayarak ön bilgi olarak sunmaktadır. Kısıtlı sayıda in vitro çalışmada fonksiyonel boyun omurga ünitesinin kemik bölümünde birim şekil değişimi ve gerilme özellikleri incelenmiştir.

YÖNTEM: Bu biyomekanik ön çalışmada, strain-gage tekniği oksiput-T1 insan kadavra modelinde C4, C5 ve C6 omur cisimleri ve laminaları üzerine uygulanmıştır. Üç farklı yükleme testi (aksiyal basma, fleksiyon ve ekstansiyon eksantrik basma yükleri) statik fizyolojik durumlar altında uygulanmıştır.

BULGULAR: Omur cisminin ön bölümünün aksiyal basma ve fleksiyon yüklemesinde basma gerilmesine, ekstansiyon yüklemesinde ise çekme gerilmesine maruz kaldığını ortaya koymaktadır. Laminalardaki gerilme dağılımı ise aksiyal yükleme sırasında çekme gerilmesi, aksiyal basma ve fleksiyon yüklemelerinde ise çekme ve basma eşit şekildedir.

SONUÇ: Omur cisimleri tüm yükleme durumlarına uyumlu olarak basma veya çekme tarzında mekanik değerlerin olduğunu ve omur cisminin sagittal planda bir ucu sabit elastik çubuk özelliği gösterdiğini göstermektedir.

ANAHTAR SÖZCÜKLER: Biyomekanik, boyun omurgası, şekil değişimi, gerilme.

Correspondence Address
Hakan BOZKUŞ
VKV Amerikan Hastanesi
Beyin Cerrahisi Bölümü
Güzelbahçe S 20
80200 Nişantaşı, İstanbul, Turkey
Phone: +90 212 3112000
e-mail : hbozkus@yahoo.com

INTRODUCTION

The stability of the bony structure of the cervical spinal column is provided by ligaments, facet joints, and discs. Any damage to the bony structure may cause stability problems, and also affect the other structures. The pattern of injury in the middle and lower cervical spinal levels is primarily influenced by loads directly applied to the vertebrae or through a lever arm of several adjacent segments. [1,2,3] However, it is still not clear what the physiological strain and stress distribution on the bony parts of the cervical spine are.

The high incidence of injury and the failure rate of the anterior fixation at the middle and lower segments of the cervical spinal column indicate that investigation of the stress distribution in this region is required. Additionally, ergonomic studies have showed that even changing the head posture away from stationary can significantly effect the load distribution at these levels. [4, 5, 6, 7, 8, 9]

Load-bearing capability of the cervical spinal columns have been analyzed with various engineering techniques in previous cervical trauma models. These techniques include pressure transducer, load cell, pressure film and finite element analysis. [10,11,12,13] The strain gage technique has also been used in single cervical vertebra or for functional spinal unit models. [14,15,16]

Although some investigators have obtained in vivo strain measurements from vertebrae in animal models, it was not possible to make long-term measurements from living bone and it was also not possible to simulate static loading without forces generated by muscle activation. [17,18] The comparison of results of the strain measurements on in vivo and in vitro bones strain has demonstrated that strain differences occur under 5%. [19]

Any mechanical strain in the vertebral surface can produce a measurable change in an electric resistance strain gage and the stresses at this point can be calculated from the strain data indirectly. This principle may help to determine the load transmission paths through the entire cervical spine.

In this pilot study, we hypothesized that determination of the distribution of in vitro normal strains and normal stresses under static physiologic loading conditions can help us understand the passive stability of the entire cervical spine model.

MATERIALS AND METHODS

Specimen preparation

The cervical spine model (Occiput-T1) of a 61-year-old embalmed cadaver who had died from pulmonary emboli six months ago was obtained. The cervical spine was dissected from the skull base and thorax, and was carefully cleaned of muscular tissue while all ligaments, joint capsules, and discs were kept intact. The specimen was examined radiographically to exclude pathology or spinal deformity (Figure 1). The specimen was wrapped in a plastic bag and stored at 4 °C before testing and after the strain gage implantations. All testing process including strain-gage implantation was performed in two days. The specimen was kept at room temperature for two hours before testing.

A 1-cm2 middle surface area of the vertebral corpuses of C4, C5 and C6 were cleaned from anterior longitudinal ligament and periosteum. The bone surfaces were smoothed with a 1-mm diamond high-speed drill (Hilan, Aesculap AG&Co.KG, Tuttlingen, Germany) under the operative microscope (Leica M841, Leica Microsystems, Wetzlar, Germany) to allow placement of the strain gages. Similarly, bilateral laminae of these levels were cleaned from soft tissues and the bone surface was smoothed in the same fashion. Care was taken not to damage facet capsules and other ligaments during this procedure.

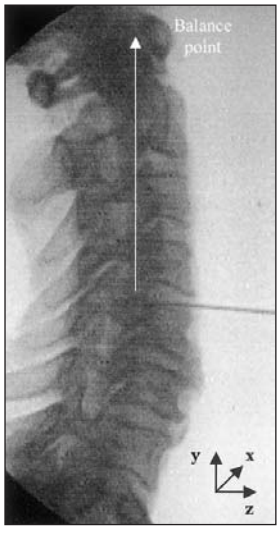

Figure 1: Lateral radiograph of the specimen. The needle marked the point of the posterior longitudinal ligament at the C5 vertebra for determining balance point of the specimen. (Reference frame was shown at the corner.

The specimen was firmly embedded in a 15-cm diameter plastic fixture with polyester resin, occiput

superiorly and T1 inferiorly. Two crossed 3-mm Kirchner wires were inserted horizontally to both ends of the specimen before embedding.

The related bone surfaces were dried with sponges and were then sanded with a thin grit emory cloth. The surface was dried with recurrent applications of the chloroform-methanol solution. Following neutralization with acidic and alkaline solutions (M-Prep Conditioner A and M-Prep Neutralizer 5, Vishay Micro-Measurements, Raleigh, NC, US), methyl- 2-cyanoacrylate (M-bond 200 Adhesive, Vishay Micro-Measurements) was applied to the bone surfaces, and allowed to cure for half an hour.

Gage selection and installation

A foil type electric resistance strain-gage rosette was chosen (SR-4 strain gages, FSEX3-03-12-S6EC, BLH Electronics, Canton, MA, US). A total of 9 rosette strain gages were used. Strain gages were bonded to the bone surface according to previous literature. [20] The grid size of the gage was 0.79 mm long by 0.4 mm wide. Gage resistance was 120W with self-temperature compensation and the gage factor was 1.99±2%. Each element of the rosette stacked 45° to the neighboring element. The gage backings were cleaned with toluene solvent and alkaline surface cleaner (M-Prep Neutralizer 5, Vishay Micro-Measurements). Methyl-2-cyanoacrylate (M-bond 200 Adhesive, Vishay Micro-Measurements) was applied on the prepared bone surface and the catalyst (M-bond 200 Catalyst, Vishay Micro-Measurements) was dropped on the backing side of the gages. The gage was bonded with the aid of mild finger pressure to conform to the bone contour for 2 minutes. The fine lead wires were attached parallel to each other along both base sides of the gage with the aid of a magnifying loop. No coating material was used and the gages were allowed to cure overnight in the refrigerator at 4°C. All gages were oriented with their axis in the craniocaudal direction of the spinal column. This allowed measuring principle strains and calculating principle stresses at the +xy plan during all loading conditions (Figures. 2, 3).

The terminals were attached on an inverse U shaped plastic frame and this was fixed to C1 (Figure 2). This helped to locate the terminals as close as possible to the related vertebral levels. The terminals were trimmed to six tabs for each rosette. The uncoated copper wires completed the connection between gage and terminals allowing maximum flexibility. The lead wires from the terminal to the wheatstone bridge was 28-gauge Teflon-coated copper with 65 strands, and each gage was connected via the quarter bridge method.

Figure 2: Photograph shows experimental setup for axial compressive loading. All gages were connected to terminals with copper cables. (Reference frame was shown at the corner).

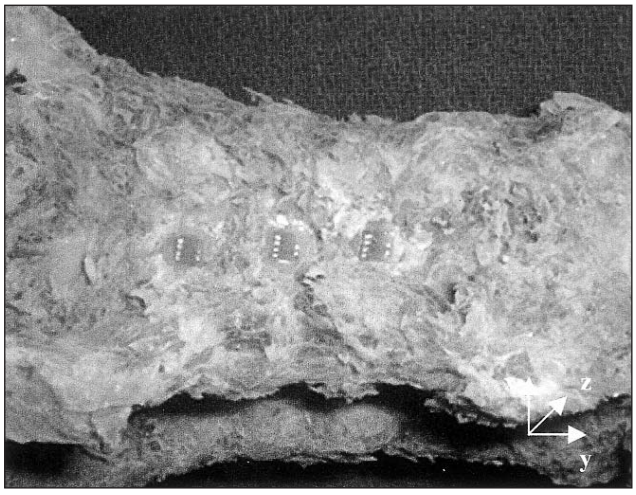

Figure 3: Photograph shows the localization of the strain gages on the left lamina sides before soldering of the lead wires. (Reference frame was shown at the corner).

Biomechanical testing

After preparation, the specimen was tested on an electro-hydraulic materials testing system (Universal Material Testing Machine Model, Tecquipment Ltd.,

U.K). The upper fixture of the specimen was kept unconstrained and horizontal to the base of the testing device. The lower fixture was fixed to the frame of the testing device (Figure 2). This left seven mobile vertebrae (C1-C7) and five mobile discs (C2-3 through C7-T1) and allowed normal cervical lordosis of the specimen during testing. The point on the upper fixture was marked as a balance point, which was determined according to the posterior longitudinal ligament (PLL) localization of C5 level before testing. This was done by fixing an 18-gauge lumbar puncture needle through the C4-5 disc space. The perpendicular line through the tip of the needle was assumed to be the balance point as used previously in the literature (Figure 1). [16] This needle was later removed before testing. The upper fixture was marked 5 cm anterior, and posterior sides of the balance point for eccentric loadings. The balance point was also confirmed with no angular motion after applying 50 N axial compressive loading.

The specimen was axially compressed at a constant velocity of 0.25 mm/sec until 50 N of maximum load was applied. The choice of 50 N was based on a simulation of static-loading conditions which could be achieved for a man standing.

The piston of the testing device was permitted to travel 10 cm before contacting the upper fixture to obtain the preset constant velocity. The maximum eccentric loads (±2.5 Nm) were achieved with the same constant velocity and the same compressive load. The specimen was immediately unloaded after maximum load or moments were reached. No failure was seen during the test.

The sequence of loading and unloading after axial compression of the specimen was flexion and extension bending with 5 cm eccentricities anterior and posterior to the reference line. To avoid problems during the final data collection due to viscoelastic effects, the test was performed after three preconditionings with a 60 sec resting period, and the actual data was then collected.

The load and displacement data of the piston were collected as a function of time with a custom-made load transducer and a custom-designed linear displacement transducer, coupled to the piston of the testing device.

The load and strain data were collected at 100 Hz per channel using a digital data acquisition system (Esam Traveller Plus, Computer Controlled Signal Condition Amplifier System, Esa-Messtechnik Gmbh, Germany).

The strain gages were calibrated with electronic shunt calibration once and balanced before the test.

RESULTS

Strain distribution

The resistance change in each strain gauge was converted to principal tensile and principal compressive microstrain (me) and was showed with specific theta angles (Figures 4, 5, 6). The positive

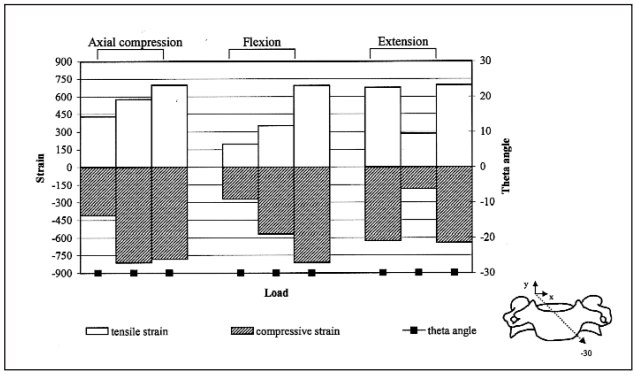

Figure 4: Bar chart representation of principal tensile and principle compressive strains at the vertebra bodies after 50 N axial compression, ±2.5 Nm flexion and extension loadings with theta angles. (The theta angle of the principal strains on the vertebra body was shown on the illustrative drawing).

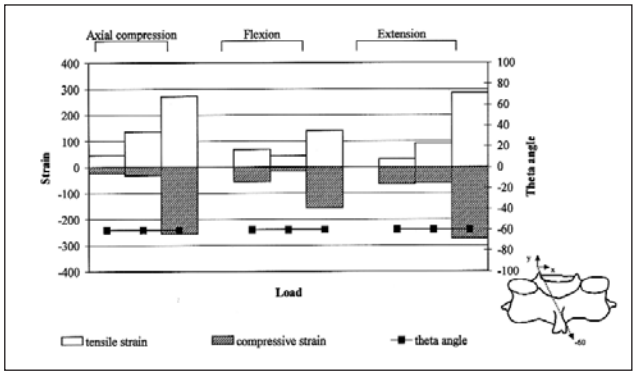

Figure 5: Bar chart representation of principal tensile and principal compressive strains at the right laminas after 50 N axial compression, ±2.5 Nm flexion and extension loadings with theta angles. (The theta angle of the principal strains on the lamina was shown on the illustrative drawing).

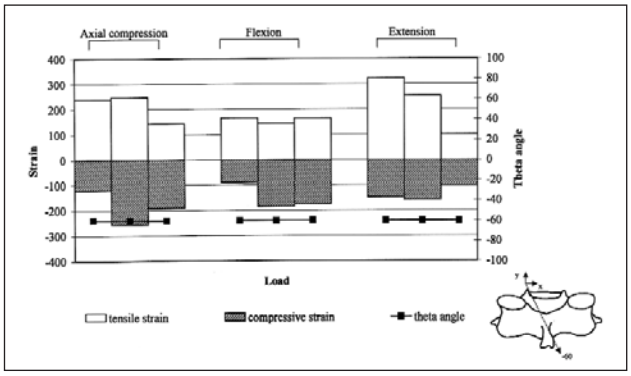

Figure 6: Bar chart representation of principal tensile and principal compressive strains at the left laminas after 50 N axial compression, ±2.5 Nm flexion and extension loadings with theta angles. (The theta angle of the principal strains on the lamina was shown on the illustrative drawing).

principal strain results indicate the tensile strain whereas negative principal strain results indicate the compressive strain. All principal strains on the vertebral bodies were oriented within –30° (theta angle) cranial caudal axis, and were oriented within –60° (theta angle) cranial caudal axis on the laminae sides.

The tensile and compressive principal strains under maximum 50 N axial and eccentric loadings (±2.5 Nm) were summarized in Table I.

Strains on the vertebrae bodies

The mean principal strains at the anterior vertebral bodies varied from –667 me (compressive) to 568 me (tensile) (Figure 4).

The maximum compressive principal strain during axial compressive loading was seen at the C5 vertebra body (-811 me). The maximum compressive principal strains during flexion and extension loading were seen at the C6 vertebra body (-812 me in flexion, –641 me in extension). The maximum tensile principal strains in all loading conditions were seen at the C6 vertebra body with similar values (range from 693me to 697 me).

The mean compressive principal strains during axial compressive and flexion loadings were superior to the mean principal tensile strains in all levels (range from –429 me to –811 me in axial compression, range from –272 me to –812 me in flexion). During extension loading, the mean tensile principal strains were superior to the mean compressive principal strains (rage from 286 me to 697 me).

Strains on the right laminas

The mean right lamina principal strains ranged from –65 me (compressive) to 152 me (tensile) (Figure 5).

Maximum compressive and tensile principal strains in all loading conditions were seen at right C6 lamina (range from –155 me to –274 me in compressive, range from 140 me to 284 me in tensile).

The mean tensile principal strains on the right laminas were superior to the mean compressive principal strains during axial compression and

Table I: Main strain pattern of the various parts of the vertebrae during axial compressive, flexion and extension loadings.

Side of the vertebra	*Type of strain*	*Loading mode*		
		Axial compressive	Flexion	Extension
Body	Compressive	C5	C6	C6
	Tensile	C6	C6	C6
	Overall	Compressive>Tensile	Compressive>Tensile	Tensile>Compressive
Right Lamina	Compressive	C6	C6	C6
	Tensile	C6	C6	C6
	Overall	Tensile>Compressive	Tensile>Compressive	Compressive>Tensile
Left Lamina	Compressive	C5	C5	C5
	Tensile	C4	C4	C4
	Overall	Tensile>Compressive	Tensile>Compressive	Tensile>Compressive

flexion loading (range from 84 me to 152 me in tensile, range from –65 me to -103 me in compressive). The mean compressive and tensile principal strains on the right laminas were similar during extension (- 133 me and 135 me).

Strains on the left laminas

The mean left lamina principal strains ranged from –189 me (compressive) to 225 me (tensile) (Figure 6).

The maximum compressive principal strains were seen on left C5 lamina in all loading conditions (range from –158 me to –256 me). The maximum tensile principal strains were seen at left C5 (247 me) during axial compressive loading, at left C4 during flexion (164 me) and at left C4 lamina during extension loading (322 me).

The mean tensile principal strains on the left laminas were superior to the mean compressive principal strains in all loading conditions (range from 157me to 225 me in tensile, range from –136 me to -189 me in compressive).

Stress distribution

The principal stresses of the specimen were calculated at the strain gage planes (xy) on which the shear stresses are zero. The positive principal stress results indicate the tensile stress whereas negative principal stress results indicate the compressive stress. All principle stresses on the vertebrae bodies were oriented within –30° (theta angle) cranial caudal axis, and were oriented within –60° (theta angle) cranial caudal axis on the laminae sides.

The stress values were calculated by planar Hooke's Law. The bone material was assumed to be linear elastic and isotropic within the strain-gage plane. The principal axes of stress and strain fields have thus coincided. The material properties used were 8.9 Gpa for Young's Modulus of the cortical bone and 0.29 for the Poisson's Ratio.

The tensile and compressive principal stresses under 50 N axial and eccentric loading (±2.5 Nm) were summarized in Table II.

Axial compression

The mean compressive principal stress on the vertebral corpuses was –8.08 MPa, and the mean tensile principal stress was 7.40 MPa. The compressive principal stress was the highest at C5 and C6 vertebra bodies (-9.51 at C5 and 9.56 MPa at C6) and the tensile principal stress was the highest at the C6 vertebra body (8.97 MPa) (Table III).

The mean compressive principal stress on the laminae was –1.42 MPa at the right side, and –2.42 MPa at the left side. The mean tensile principal stress on the laminae was 1.76 MPa at the right side, and 2.56 MPa at the left side. Maximum compressive and tensile principal stresses on the laminae were seen at the C5 and C6 levels with similar values (–3.18 MPa at the left C5 side, –3.23 MPa at the right C6 and 3.12 MPa at the left C5 side, 3.35 MPa at the right C6 side).

Table II: Main stress pattern of the various parts of the vertebrae during axial compressive, flexion and extension loadings.

Side of the vertebra	*Type of strain*	*Loading mode*		
		Axial compressive	Flexion	Extension
Body	Compressive	C5, C6	C4, C6	C4, C6
	Tensile	C6	C4, C6	C4, C6
	Overall	Compressive>Tensile	Compressive>Tensile	Tensile>Compressive
Right Lamina	Compressive	C6	C6	C6
	Tensile	C5	C6	C6
	Overall	Tensile>Compressive	Compressive>Tensile	Compressive>Tensile
Left Lamina	Compressive	C6	C5, C6	C4, C5
	Tensile	C5	C4, C5, C6	C4
	Overall	Tensile>Compressive	Compressive>Tensile	Compressive>Tensile

Table III: Tensile and compressive principal stresses (MPa) under maximum 50N axial compression, ±2.5 Nm flexion and extension loadings. Mean values were indicated in the parenthesis.

	Tensile stresses (MPa)			Compressive stresses (MPa)		
	Axial C	*Flexion*	*Extension*	*Axial C*	*Flexion*	*Extension*
C4 corpus	5.33	9.02	8.33	-5.18	-9.85	-7.98
C5 corpus	7.90	5.02	3.30	-9.51	-6.51	-2.58
C6 corpus	8.97	9.02	8.58	-9.56	-9.85	-8.19
mean	*(7.40)*	*(7.68)*	*(6.73)*	*(-8.08)*	*(-8.73)*	*(-6.25)*
C4 right lamina	0.52	0.80	0.49	-0.36	-0.72	-0.72
C5 right lamina	1.42	0.38	1.06	-0.69	-0.20	-0.84
C6 right lamina	3.35	1.80	3.53	-3.23	-1.90	-3.46
mean	*(1.76)*	*(0.99)*	*(1.69)*	*(-1.42)*	*(-0.94)*	*(-1.67)*
C4 left lamina	2.64	1.84	3.55	-1.84	-1.33	-2.35
C5 left lamina	3.12	1.92	2.61	-3.18	-2.21	-2.25
C6 left lamina	1.92	2.08	1.27	-2.25	-2.16	-1.28
mean	*(2.56)*	*(1.94)*	*(2.47)*	*(-2.42)*	*(-1.90)*	*(-1.96)*

During axial compressive loading, the mean compressive principal stress on the vertebral bodies was superior to tensile principal stress (-8.08 MPa to 7.40 MPa). However, the mean tensile principal stresses were superior to the mean compressive principal stresses on both lamina sides (1.76 MPa to –1.42 MPa at the right side, 2.56 MPa to –2.42 MPa at the left side).

Anterior eccentric compression (flexion)

The mean compressive principal stress on the vertebral corpuses was –8.73 MPa, and the mean tensile principal stress was 7.68 MPa at this side. The compressive and tensile principal stresses were the highest at the C4 and C6 vertebral bodies (-9.85 MPa compressive, 9.02 MPa tensile) (Table III).

The mean compressive principal stress on the laminae was –0.94 MPa at the right side, and –1.90 MPa at the left side. The mean tensile principal stress on the laminae was 0.99 MPa at the right side, and 1.94 MPa at the left side. The maximum compressive principal stresses were seen at the right C6 lamina (-1.90 MPa) and left C5 and left C6 lamina levels (-2.21 MPa at C5, -2.16 MPa at C6). The maximum tensile principal stresses were seen at the right C6 lamina (1.80 MPa) and all left laminae (range from 1.84 MPa to 2.08 MPa).

During flexion loading, the mean compressive principal stress on the vertebra bodies was superior to the mean tensile principal stress (-8.73 MPa to 7.68 MPa). The mean compressive and the mean tensile principal stress on both laminar sides were similar (-0.94 MPa to –0.99 MPa at the right side, -1.90 MPa to 1.94 MPa at the left side).

Posterior eccentric compression (extension)

The mean compressive principal stress on the vertebral corpuses was –6.25 MPa, and the mean tensile principal stress was 6.73 MPa on this side. The compressive principal stress was the highest at C4 and C6 vertebra body (-7.98 at C4 and -8.19 MPa at C6) and the tensile principal stress was the highest at C4 and C6 vertebral bodies (8.33 MPa at C4, 8.58 MPa at C6) (Table III).

The mean compressive principal stress on the laminas was –1.67 MPa at the right side, and –1.96 MPa at the left side. The mean tensile principal stress on the laminas was 1.69 MPa at the right side, and 2.47 MPa at the left side. The maximum compressive principal stresses on the laminar sides were seen at the right C6 level (–3.46 MPa), and the left C4 and C5 levels (-2.35 at C4 and -2.25 MPa at C5). The maximum tensile principal stresses on the laminar side were determined at the right C6 level (3.53 MPa), whereas it was seen at the left C4 level (3.55 MPa).

During extension loading, the mean tensile principal stress on the vertebral bodies was superior

to the mean compressive principal stress (6.73 MPa to –6.25 MPa). The mean compressive and the mean tensile principal stresses on both laminar sides were similar (-1.67 MPa to 1.69 MPa at the right and -2.47 MPa to –1.96 MPa at the left).

DISCUSSION

In this study, 50 N loading was chosen to permit repeated application of load to the specimen without fracture and to also simulate normal head weight. We have analyzed stress measurement rather than bony failure and the following hypotheses therefore consider only our particular specimen model.

Under axial compressive loading, compressive and tensile stresses were cumulated especially on the C5 and C6 vertebral bodies and laminae. Although compressive stress was dominant on the vertebral bodies, the tensile stress was main stress on the both laminar sides. Because of the cervical spine curvature, these stress results may explain why any possible bone failure after axial loading will occur with a high incidence at C5 and C6 levels. The C4 vertebra body has similar compressive and tensile stress with smaller amounts than other levels. This pattern leads us to postulate that the C4 vertebral body is relatively spared from axial loading.

Anterior and posterior eccentric compressive loadings produced maximum compressive and tensile stress at the C4 and C6 vertebral bodies. The C5 vertebra body suffered relatively little compressive and tensile stress during these loading conditions. During flexion and extension movement, a moment arm creates reverse mechanical response at the vertebral bodies. The compressive stress on the vertebral bodies was dominant during flexion whereas the tensile stress on the vertebral bodies was dominant during extension. Both types of stress were equal on both laminar sides during eccentric loadings.

Different quantitative comparative results of the mean tensile and the compressive stresses on the laminas during anterior and posterior eccentric compressive loading indicate that a possible coupling motion causes different amount of stresses over laminae. However the overall stress trend was same at both sides of the laminae.

The compressive and tensile stress shielding effect of the C5 vertebra body in both eccentric loading conditions also point out that this level acts as a center of rotation in the sagittal plane. This is a point that transmits stress to the cranial and caudal sides of the spine during bending with little stress effect on itself. On the other hand, this level carries compressive stress during axial loading. This explanation carries similarity to the Euler`s theory of columns. [21] According to this theory, the bending of a beam is directly proportional to its length but is inversely proportional to its elastic modulus and moment of inertia. As determined in our study, the cervical spine can carry more stress in axial compression loading than both eccentric loading conditions. Although the length and the elastic modulus of the spine are constant in each loading mode, the moment of inertia increases during eccentric loadings by the effect of the moment arm. In this pilot study, this feature was first demonstrated by stress distributions in a full-length cervical spine model.

Overall compressive stress results have shown that vertebral bodies can transmit more stress than laminae. This was 4 times more in axial compression, 6 times more in flexion and 3 times more in extension loading. Additionally, vertebral bodies have been capable of transmitting 3 to 4 times more tensile stress than the laminae.

All principal strain and stress patterns at vertebra bodies were determined within -30∞ along the craniocaudal axis of the spine. Nevertheless, the patterns at the laminae were determined within -60°. This theta angle difference should be considered with the orientation of the cortical bone surfaces on the reference frame and also the cortical bone quality at both sides.

Comparison with previous studies.

Previous studies concerning the cervical vertebral strain and stress analyses have been performed on functional spinal unit models. [15,16] The disadvantage of these models is that an entire cervical spine model has a wide range of motion accompanied by a significant amount of coupling motions. [22] Additionally, the laminar sides were preferred to the lateral mass sides for strain gage applications in the present study, thus avoid damaging facet capsules.

Pintar et al. [16] have determined the patterns of localized strains in the C6 or C7 vertebra model. They concluded that the anterior vertebral body experienced tensile strains with posterior loading eccentricities and compressive strains with anterior eccentricities, whereas the lateral masses experienced almost entirely compressive strains throughout the loading sequence. Similar results were seen in vertebral bodies in the present study. Moreover, maximum compressive strains especially occurred on the C5 vertebral body in axial loading and C6 vertebral body during both eccentric loadings. Lamina strains were determined as mainly being the tensile pattern during all loading conditions except that the right lamina sides showed equal tensile and compressive strain during extension loading. It is impossible to compare the lateral mass results of Pintar et al. [16] with our lamina results but it may be speculated that the compressive strains on the lateral masses convert in some way to tensile strain pattern at the lamina sides.

Cripton [15] has reported that flexion and 'flexion with preload' loading modes resulted in compressive force in the anterior column and tensile forces in the posterior column. Extension loading resulted in compression force at the posterior column and tensile force in the anterior column. Extension with preload caused compressive forces in both columns.

Our stress results have parallelism with the load-sharing study of Cripton. [15] The results of the present study suggest that, axial compressive and flexion loading modes have resulted in compressive stress pattern at the anterior column while there was a tensile stress pattern at the anterior column during extension loading. In the present study, laminar stress was tensile during axial loading but the tensile and compressive stresses were equal during flexion and extension loadings. We cannot demonstrate compressive stress patterns on the posterior column during extension. We believe that more than one rosette strain gage for each laminar side might be necessary to determine the real stress on the laminar sides.

Study limitations.

The present study has limitations imposed by using the embalmed and aged cadaver specimen. The effect of different embalming solutions on the strain properties of bone has been reported. Embalming causes a significant reduction in the ultimate compressive strength, but only a very slight reduction in the ultimate tensile strength, maximum strain (3.4% reduction from unembalmed for maximum tensile strain, 4.4 % reduction from unembalmed for maximum compressive strain) and modulus of elasticity. [23] Although all strain results were obtained in the linear elastic region and the ultimate strength of the bone was not tested in our study, it should be taken in consideration that the results were in the ±3.4-4.4% accuracy range.

The use of aged cadaver limits the results of this study's applicability to younger age group. However, the main emphasis was to simulate the strain and stress distribution in the bony components of the vertebrae under static physiologic loading. The strain and stress patterns associated with a young specimen could be expected to show a similar trend.

The other limitation is that the single specimen (n=1) does not lend itself to statistical comparisons. However, the result of single specimen can demonstrate overall strain and stress patterns. This has been confirmed in the literature. [15]

This study was provided initial pilot results of the load-strain and the load-stress of the entire cervical spine under quasi-static, controlled, sagittal symmetrical loading conditions. Axial rotation and lateral bending conditions were not investigated in this research. These loadings need adequate angular displacement measurements during these tests and this was not possible in our testing setup.

CONCLUSION

The anterior vertebral body experienced compressive stress with axial compressive and flexion loadings and tensile stress with extension loading. Laminar stresses were tensile pattern during axial compressive loading while tensile and compressive stresses were equal during flexion and extension loadings. The C5 vertebral body carries compressive stress during axial loading but demonstrates a stress conduction effect during eccentric loadings.

APPENDIX

Basic strain gage technique principles for experimental stress analysis were shown in Figure Appendix 1.

For two-dimensional stress analysis, such as at a point P on the surface of a body, the general stress components are, σ_{xx} ,σ_{yy} and τ_{xy} at the point. These stress components, are directly linked to the strain values, ε_{xx} , ε_{xy} and γ_{xy} . For materials that are assumed to be linear elastic, the law (formerly named the constitutive equation for a material) are known as the Hooke's Law for two-dimensional stress and strain field.

Thus, for any point P, the strain, and relatedly the stress field can be determined by measuring the strains. The strain filed has three parameters to be determined (ε_{xx} =,ε_{yy} and γ_{xy}). At a point P, the strain in any direction can be expressed as

$$\varepsilon_{aa} =,\varepsilon_{xx}\cos^2 \text{ and } \gamma_{xy}+\alpha_a+\varepsilon_{yy}\sin^2\alpha_a+\gamma_{xy}\cos\alpha_a\sin\alpha_a$$

By measuring strain components in three distinct directions (ε_{aa},ε_{bb} and ε_{cc}) whose orientations are predefined (with α_a , α_b and α_c - see Figure Appendix 1- arrows denoting the positive direction), the strain (thus stress) field can be determined experimentally utilizing the solution of three linear algebraic equations in three unknowns.

Any stress or strain field at point P can be expressed, by rotating the xy axis system about point P, in terms of principal stresses and/or strains whose directions coincide, for isotropy, within the measuring plane. For ε_{aa} to be a principal strain, α_a should be such that, for the rotated $x_a y_a$ coordinate system, the shearing strain by the infinitesimal element should vanish. The graphical utilization of this fact is known as the Mohr's Circle for stress and strain fields in mechanics, used for defining the strain (stress) field in any direction (Figure Appendix 2).

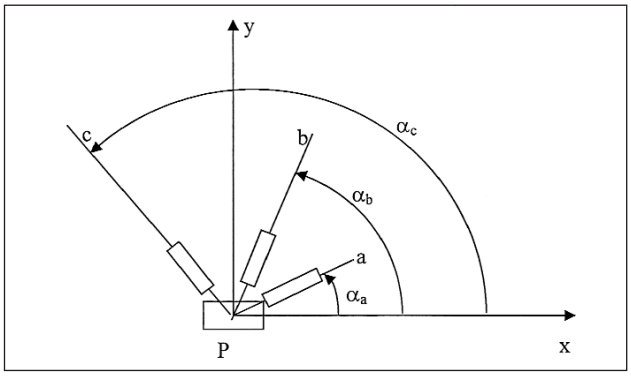

Figure Appendix 1: The axis system and orientation principles of three strain gages in three predefined directions (a,b and c) for determining planar strain and stress fields at point P by experiment.

Notice that, the xy axis system at a point P is defined independently of the axis system that defines the orientation of the complete structure, which within this text is the cervical column and the Oxyz axis system.

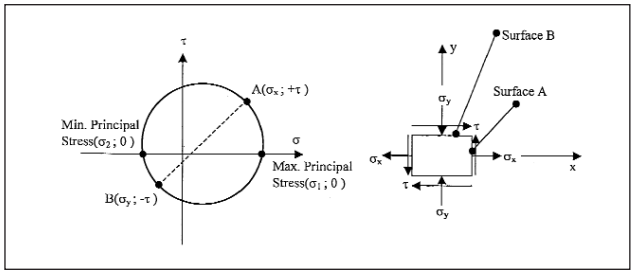

Figure Appendix 2: Mohr's Circle representation of a two-dimensional stress field on an infinitesimal element is shown. Points A and B denote two perpendicular surfaces of the element, and re

References

1. Cusick JF, Yoganandan N. Biomechanics of the cervical spine 4: major injuries. Clin Biomech 17: 1-20, 2002
2. Sances A Jr, Myklebust JB, Maiman DJ, Larson SJ, Cusick JF, Jodat RW. The biomechanics of spinal injuries. Crit Rev Biomed Eng 11; 1-75, 1984
3. Shono Y, McAfee PC, Cunningham BW. The pathomechanics of compression injuries in the cervical spine. Nondestructive and destructive investigative methods. Spine 18: 2009-2019, 1993
4. Althoff I, Brinckmann P, Frobin W, Sandover J, Burton K. An improved method of stature measurement for quantitative determination of spinal loading. Spine 17: 682-693, 1992
5. Bonney RA, Corlett EN. Head posture and loading of the cervical spine. Applied Ergonomics 33: 415-417, 2002
6. Isomi T, Panjabi MM, Wang JL, Vaccaro AR, Garfin SR, Patel T. Stabilizing potential of anterior cervical plates in multilevel corpectomies. Spine 21: 2219-2223, 1999
7. Koh YD, Lim TH, You JW, Eck J, An HS. A biomechanical comparison of modern anterior and posterior plate fixation of the cervical spine. Spine 26: 15-21, 2001
8. Rapoff AJ, O`Brien TJ, Ghanayem AJ, Heisey DM, Zdeblick TA. Anterior cervical graft and plate load sharing. J Spinal Disord 1: 45-49, 1999

9. Sasso RC, Ruggiero RA, Reilly TM, Hall PV. Early reconstruction failures after multilevel cervical corpectomy. Spine 28: 140-142, 2003

10. DiAngelo DJ, Foley KT, Vossel KA, Rampersaud YR, Jansen TH. Anterior cervical plating reverses load transfer through multilevel strut-grafts. Spine 7: 783-795, 2000

11. Goel VK, Clausen JD. Prediction of load sharing among spinal components of a C5-6 motion segment using the finite element approach. Spine 23: 684-691, 1998

12. Ng HW, Teo EC, Lee KK, Qiu TX. Finite element analysis of cervical spinal instability under physiologic loading. J Spinal Disord 16: 55-65, 2003

13. Smith TJ. In vitro spinal biomechanics. Experimental methods and apparatus. Spine 16: 1204-1210, 1991

14. Bozkus H, Bozdag E, Hanci M, Uzan M, Sarioglu AC. Surface strain distribution on C1 during quasistatic axial compressive loading. Eurobiomechanics 2000, Aug 27-Sep 3, 2000, Dublin, Ireland

15. Cripton PA. Load sharing in the human cervical spine. (Thesis). Quenn`s University Press, Canada, 1999

16. Pintar FA, Yoganandan N, Pesigan M, Reinartz J, Sances A Jr, Cusick JF. Cervical vertebral strain measurements under axial and eccentric loading. J Biomech Engin 117: 474-478, 1995

17. Lanyon LE. In vivo bone strain recorded from thoracic vertebrae of sheep. J Biomech 5: 277-281, 1972

18. Lanyon LE. Strain in sheep lumbar vertebrae recorded during life. Acta Orthop Scand 42: 102-112, 1971

19. Cochran GVB. Implantation of strain gages on bone. Technical note. J Biomech 5: 119-123, 1972

20. Buttermann GR, Kahmann RD, Lewis JL, Bradford DS. An experimental method for measuring force on the spinal facet joint: Description and application of the method. J Biomech Eng 113: 375-386, 1991

21. Crisco JJ, Panjabi MM. Euler stability of the human ligamentous lumbar spine: Part I Theory. Clin Biomech 7: 19-26, 1992

22. Panjabi MM, Crisco JJ, Vasavada A, Oda T, Cholewicki J, Nibu K, Shin E. Mechanical properties of the human cervical spine as shown by three-dimensional load-displacement curves. Spine 26: 2692-2700, 2001

23. McElhaney J, Fogle J, Byars E, Weaver G. Effect of embalming on the mechanical properties of beef bone. J Appl Physiol 19: 1234-1236, 1964